JACS
JOURNAL OF THE AMERICAN CHEMICAL SOCIETY
pubs.acs.org/JACS
Article

A $4H^+/4e^-$ Electron-Coupled-Proton Buffer Based on a Mononuclear Cu Complex

Tong Wu, Khashayar Rajabimoghadam, Ankita Puri, David D. Hebert, Yi Lin Qiu, Sidney Eichelberger, Maxime A. Siegler, Marcel Swart,* Michael P. Hendrich,* and Isaac Garcia-Bosch*

Cite This: J. Am. Chem. Soc. 2022, 144, 16905−16915
Read Online
ACCESS | Metrics & More | Article Recommendations | Supporting Information

ABSTRACT: In this research article, we describe a $4H^+/4e^-$ electron-coupled-proton buffer (ECPB) based on Cu and a redox-active ligand. The protonated/reduced ECPB (complex **1**: $[\mathbf{Cu(8H^+/14e^-)}]^{1+}$), consisting of Cu^I with 2 equiv of the ligand ($^{cat}LH_4$: 1,1′-(4,5-dimethoxy-1,2-phenylene)bis(3-(*tert*-butyl)-urea)), reacted with H^+/e^- acceptors such as O_2 to generate the deprotonated/oxidized ECPB. The resulting compound, (complex **5**: $[\mathbf{Cu(4H^+/10e^-)}]^{1+}$), was characterized by X-ray diffraction analysis, nuclear magnetic resonance (^{1}H-NMR), and density functional theory, and it is electronically described as a cuprous bis(benzoquinonediimine) species. The stoichiometric $4H^+/4e^-$ reduction of **5** was carried out with H^+/e^- donors to generate **1** (Cu^I and 2 equiv of $^{cat}LH_4$) and the corresponding oxidation products. The **1**/**5** ECPB system catalyzed the $4H^+/4e^-$ reduction of O_2 to H_2O and the dehydrogenation of organic substrates in a decoupled (oxidations and reductions are separated in time and space) and a coupled fashion (oxidations and reductions coincide in time and space). Mechanistic analysis revealed that upon reductive protonation of **5** and oxidative deprotonation of **1**, fast disproportionation reactions regenerate complexes **5** and **1** in a stoichiometric fashion to maintain the ECPB equilibrium.

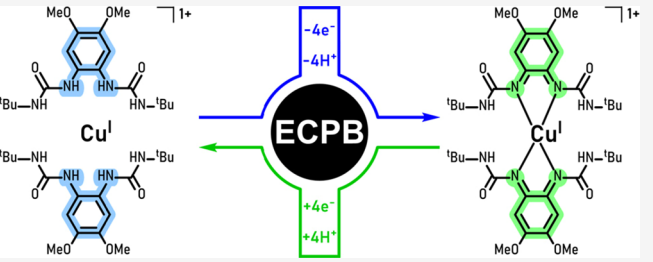

INTRODUCTION

Many important natural and industrial processes involve the transfer of multiple protons and electrons usually in a concerted fashion (i.e., proton-coupled electron transfer[1−3]), including O_2 reduction,[4] H_2O oxidation,[5] N_2 reduction,[6] H_2 formation,[7] among others.[8] Nature has developed mechanisms by which protons and electrons can be stored, transported, and released when needed. For example, the protons and electrons obtained during water oxidation in photosystem II are stored in plastoquinone (PLQ), which is protonated and reduced to plastoquinol (PLQol), and are transported to cytochrome b_6f and photosystem I to convert $NADP^+$ to NADPH (Figure 1A).[9,10] The PLQ/PLQol couple is a redox mediator that acts as an electron-coupled-proton buffer (ECPB), responding to protonating/reducing conditions by storing H_2 equivalents and deprotonative/oxidative conditions by delivering H_2 equivalents in a reversible fashion.

Inspired by these natural systems, soluble redox mediators are currently utilized in fuel and electrochemical cells.[11] Cronin and co-workers have developed ECPBs based on polyoxometalates (POM) or quinones that are used to decouple the half-reactions of electrolytic H_2O splitting into H_2 and O_2 formation (Figure 1B).[12,13] The utilization of ECPBs introduces an additional electrochemical step, which allows for separating, in time and space, the O_2 evolving reaction (OER: H_2O is deprotonated/oxidized to O_2 in the Pt electrode, and the resulting protons and electrons are utilized to protonate/reduce the ECPB) and the H_2 evolving reaction (HER: the protons and electrons stored in the ECPB are used to generate H_2 at the Pt electrode).[14] Other advantages of this setup are the relatively low operational potentials (determined by the potential difference of the ECPBs and the Pt HER and OER), the purity of the gases synthesized, and the higher durability of the cell components (e.g., the Nafion membrane is easily degraded by the reactive oxygen species that result from H_2 and O_2 mixing).

In a landmark contribution, Deng and coworkers have developed a liquid-phase fuel cell based on POMs that act as ECPBs (Figure 1C).[15] With this setup, one of the POMs ($ECPB_A$) catalyzes the oxidation of biomass in solution and delivers the H_2 equivalents to the anode. Protons and electrons are captured at the cathode by the second POM ($ECPB_B$, $E_{1/2}$ of $ECPB_B$ > $E_{1/2}$ of $ECPB_A$), which catalyzes the reduction of O_2 to H_2O. By decoupling the two redox processes and moving the catalytic process from the electrode surface to the

Received: May 23, 2022
Published: September 9, 2022

https://doi.org/10.1021/jacs.2c05454
J. Am. Chem. Soc. 2022, 144, 16905−16915

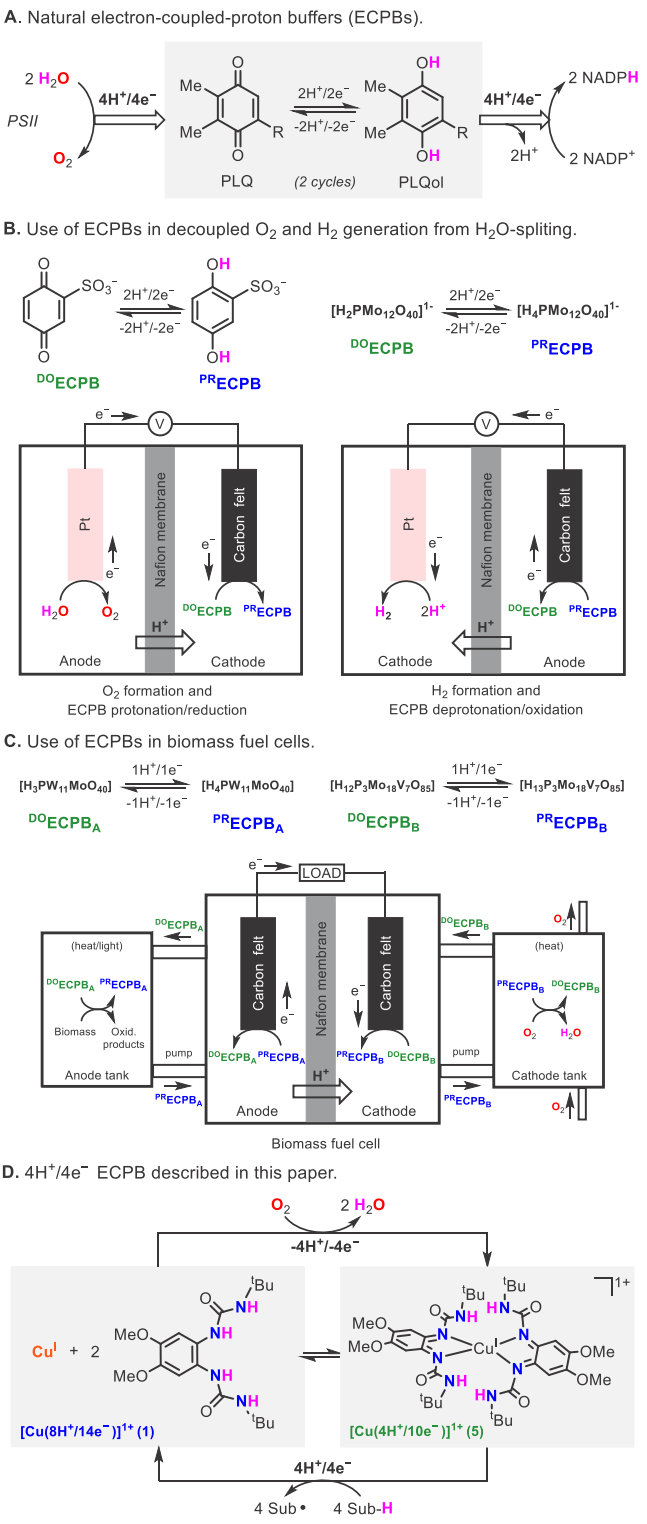

Figure 1. (A) Natural $2H^+/2e^-$ ECPB. (B) Use of ECPBs for the decoupled generation of O_2 and H_2 from H_2O splitting. (C) Use of ECPBs in biomass fuel cells. (D) $4H^+/4e^-$ ECPB based on Cu and redox-active ligands.

solution, nonmetallic electrodes could be used (cheap graphite felt), and the oxidation and reduction processes could be performed in separate tanks, which allows for applying heat and/or light to the reactive solutions.

In the present work, we describe an ECPB based on Cu and a redox-active ligand that is capable of decoupling the reductive protonation of O_2 to H_2O with the oxidative deprotonation of organic substrates in an unprecedented $4H^+/4e^-$ fashion (Figure 1D).

RESULTS AND DISCUSSION

Synthesis and Characterization of the Copper Complexes. The reaction between the ligand $^{cat}LH_4$ (1,1′-(4,5-dimethoxy-1,2-phenylene)bis(3-(*tert*-butyl)urea)) and 0.5 equiv of $[Cu^I(CH_3CN)_4](PF_6)$ in air produced the cationic complex **5**, $[\mathbf{Cu(4H^+/10e^-)}]^{1+}$ (see the Supporting Information, SI, for details on the synthesis and naming of the complexes). Based on our previous work, we prepared the dianionic complex **2**, $[\mathbf{Cu(4H^+/13e^-)}]^{2-}$, via deprotonation of $^{cat}LH_4$ with 2 equiv of KH followed by addition of 0.5 equiv of $Cu(OAc)_2$ under anaerobic conditions (Figure 2A).[16,17]

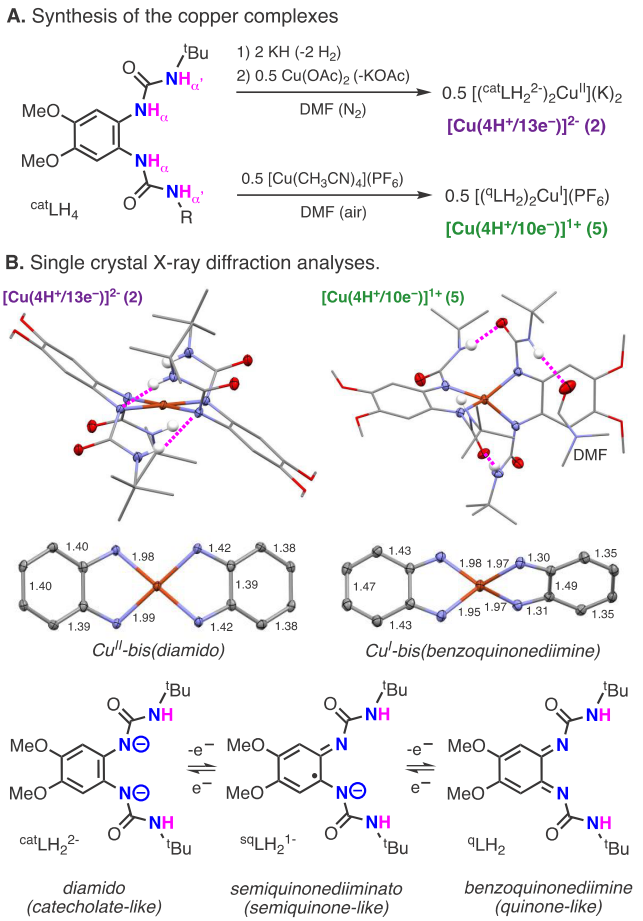

Figure 2. (A) Synthesis of complexes **2** and **5**. (B) Single crystal X-ray diffraction analyses of the complexes **2** and **5** (H-atoms, K countercations, PF_6 counteranions, and solvent molecules were omitted for clarity, see the SI for details).

Both Cu complexes were characterized by single crystal X-ray diffraction analyses (SCXRD, Figure 2B). Complex **2** adopts a square-planar geometry that is stabilized via intramolecular N−H···N H-bonding interactions between the ureanyl substituents of one of the ligands and the basic Nα of the other ligand (d(Hα'···Nα): 2.151(9)−2.20(2) Å). Analysis of the bond distances of the diamine scaffolds indicates that the two ligands in complex **2** are fully reduced (d(C−N): 1.418(2) Å), consistent with a Cu^{II} ion bound by two catecholate-like ligands (i.e., $[(^{cat}LH_2^{2-})_2Cu^{II}]^{2-}$).[16] Con-

https://doi.org/10.1021/jacs.2c05454
J. Am. Chem. Soc. 2022, 144, 16905−16915

versely, complex **5** adopted a pseudo-tetrahedral geometry in which the bond distances measured for the diamine backbone indicated that the redox-active ligand is fully oxidized (d(C−N): 1.305 (2) Å), suggesting that **5** is a Cu^{I} complex with two quinone-like ligands.[18]

Electrochemistry. In one of our previous articles, we showed that Cu complexes bearing similar ligands are able to reach five molecular oxidation states via reduction/oxidation of the metal center or the ligand scaffold.[16] Cyclic voltammetry (CV) measurements for $[\mathbf{Cu(4H^{+}/13e^{-})}]^{2-}$ (**2**) found that this complex was reversibly oxidized to three "high-valent" oxidation states, namely, $[\mathbf{Cu(4H^{+}/12e^{-})}]^{1-}$ (**3**), $[\mathbf{Cu(4H^{+}/11e^{-})}]^{0}$ (**4**), and $[\mathbf{Cu(4H^{+}/10e^{-})}]^{1+}$ (**5**) at relatively low redox potentials (from −0.5 to −0.9 V vs $Fc^{0/+}$, see Figure 3A). CV experiments using the isolated complex **5** led to identical results, suggesting that the oxidation of **2** and reduction of **5** occur via equivalent $1e^{-}$ processes.

Oxidation of **2** using stoichiometric amounts of ferrocenium hexafluorophosphate ($FcPF_6$) produced **3**, **4**, and **5** (Figure 3B). Reduction of **5** with stoichiometric amounts of $CoCp_2$ ($CoCp_2$: cobaltocene) also produced **4**, **3**, and **2** (see Figures S10−S12 in the SI). Complex **5** was characterized by ^{1}H-NMR, confirming that is diamagnetic Cu^{I} complex (S = 0). EPR measurements for **2** and **4** confirmed their paramagnetic nature (S = 1/2), with signals characteristic of a Cu-centered unpaired electron for **2** and ligand-centered unpaired electron for **4** (see Figure 3C)[19] The g_z-value (2.21) and A_z-value (14.9 mT) of the Cu^{II} center in complex **2** were typical of D_{4h} or D_{2d} coordination.[16,17] The intensity of the signals was quantitative for the amount of Cu added to form the complex. Because of the redox noninnocent nature of the ligand scaffolds, assigning the oxidation state of the metal (Cu^{I}, Cu^{II}, Cu^{III}) and the ligand scaffold ($^{cat}LH_2^{2-}$, $^{sq}LH_2^{1-}$or $^{q}LH_2$) is not trivial (see Figure 4A).[20] For example, complex **3** was EPR-silent in both perpendicular and parallel mode (S = 0), which might result from the formation of a d^8 Cu^{III} ion bound by two catecholate-like ligands ($[(^{cat}LH_2^{2-})_2Cu^{III}]^{1-}$), a d^9 Cu^{II} complex with the metal antiferromagnetically coupled with a ligand-centered radical ($[(^{cat}LH_2^{2-})(^{sq}LH_2^{1-})Cu^{II}]^{1-}$, or a d^{10} Cu^{I} center bound by two semiquinone-like ligands that are antiferromagnetically coupled $[(^{sq}LH_2^{1-})_2Cu^{I}]^{1-}$.

DFT calculations were conducted to gather insight into the electronic structure of complexes **2**, **3**, **4**, and **5** (Figure 4B). These computations included the optimization of the complexes in different geometries (D_{4h} vs D_{2d}) and different spin states (see details in section 8 of the SI). For all of the complexes, the D_{2d} structures were more stable than the corresponding D_{4h}. For complex **2**, the computed Cu···Nα, Nα···C_{Ar} and C_{Ar}···C_{Ar} distances were similar to the values measured by XRD analysis. Oxidation of complex **2** to **3**, **4**, and **5** led to a gradual increase in the computed C_A···C_{Ar} distances (from 1.40 to 1.42 Å) and decrease in the Nα-C_{Ar} distances (from 1.38 to 1.32 Å), in agreement with the proposed ligand-centered oxidations. Spin-density plots also supported this proposal (see Figure 4B). For complex **2**, the spin density was localized in the Cu and the Nα, consistent with the formulation of **2** as an Cu^{II} ion bound by two catecholate-like ligands, $[(^{cat}LH_2^{2-})_2Cu^{II}]^{2-}$. The d-orbital occupancy also suggested that the Cu center in complex **2** was a d^9 metal (note: occupancy factors lower than 0.7 indicate that the d-orbital is unoccupied[21]). Oxidation of complex **2** to **3** caused delocalization of the spin density from the Cu and Nα to the aromatic backbones and a d-orbital occupancy

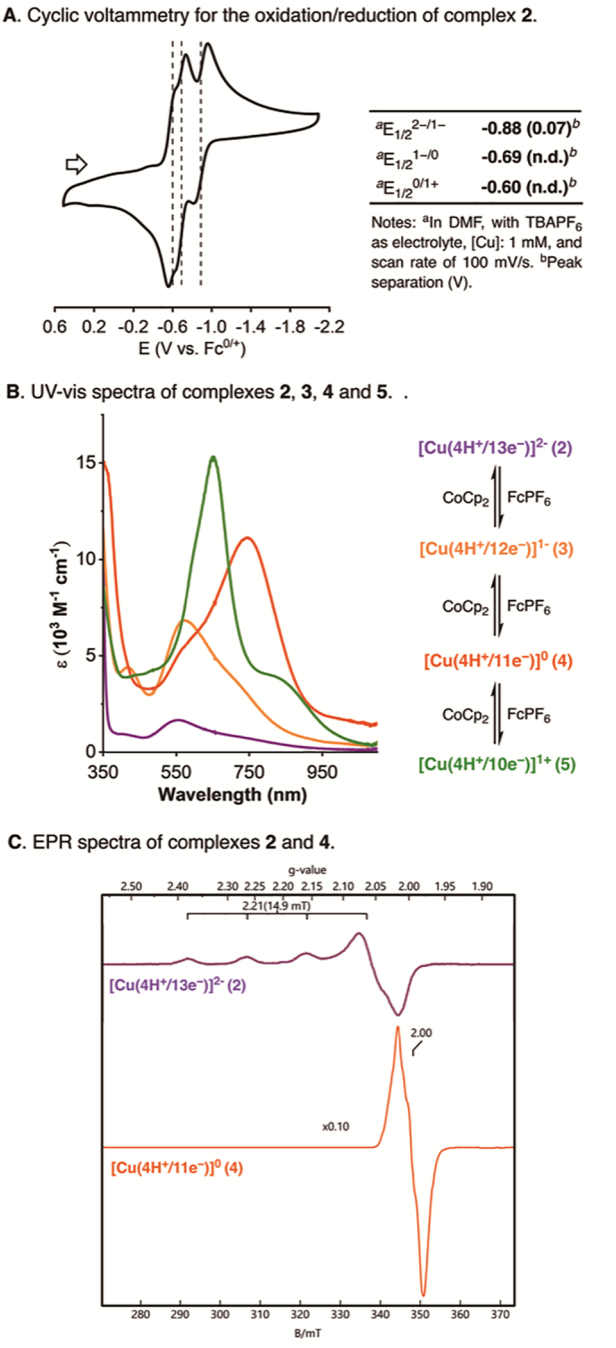

Figure 3. (A) CV measurements for the reversible oxidation/reduction of complexes **2** and **5**. (B) UV−vis spectra for the complexes **2**, **3**, **4**, and **5**. (C) EPR spectra for complexes **2** and **4**.

characteristic of a d^{10} metal. Hence, the electronic structure of complex **3** was consistent with a Cu^{I} complex containing two antiferromagnetically coupled semiquinone-like ligands $[(^{sq}LH_2^{1-})_2Cu^{I}]^{1-}$ (Note: for complex **3**, the computed singlet and triplet states had similar energy, but experimental evidence indicates that complex **3** is diamagnetic, see the SI). Oxidation of **3** to **4** led to a decrease on the spin density on one of the aromatic backbones while maintaining a d^{10} orbital occupancy, which suggested that complex **4** was a Cu^{I} system bound by a semiquinone-like and a quinone-like ligand, $[(^{sq}LH_2^{1-})(^{q}LH_2)$-$Cu^{I}]^{0}$. For complex **5**, the computed distances (similar to the ones obtained by X-ray diffraction analysis), the spin-density

https://doi.org/10.1021/jacs.2c05454
J. Am. Chem. Soc. 2022, 144, 16905−16915

A. Molecular oxidation states formed upon oxidation/reduction of complexes **2** and **5**.

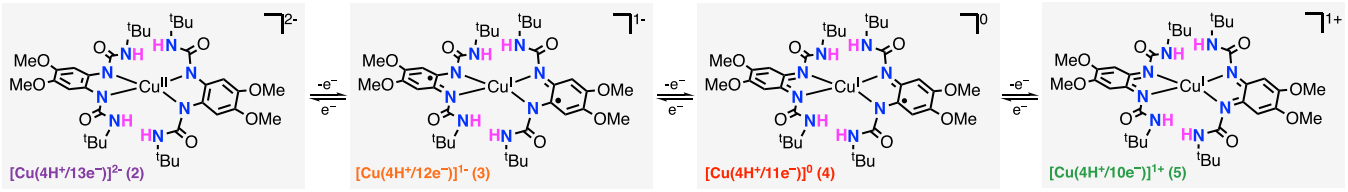

$[(^{cat}LH_2^{2-})_2Cu^{II}]^{2-}$ (S = 1/2)
XRD, EPR, UV-vis, DFT

$[(^{sq}LH_2^{1-})_2Cu^{I}]^{1-}$ (S = 0)
EPR, UV-vis, DFT

$[(^{sq}LH_2^{1-})(^{q}LH_2)Cu^{I}]^{0}$ (S = 1/2)
EPR, UV-vis, DFT

$[(^{q}LH_2)_2Cu^{I}]^{1+}$ (S = 0)
XRD, NMR, DFT

B. DFT calculations on the electronic structure of complexes **2**, **3**, **4** and **5**.

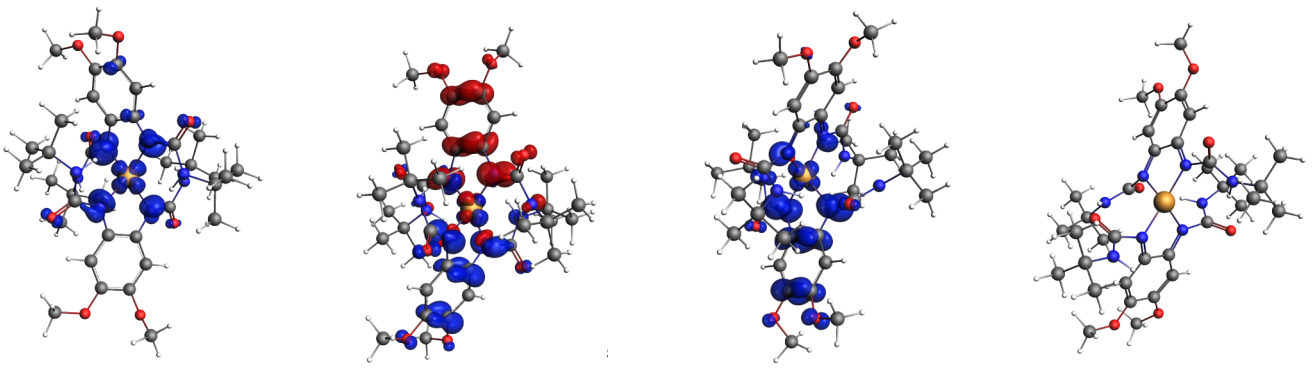

$[Cu(4H^+/13e^-)]^{2-}_{D2d}$ (2)
d(Cu···N_α) (Å): 1.97
d(N_α···C_{Ar}) (Å): 1.38
d(C_{Ar}···C_{Ar}) (Å): 1.40
<S^2> (unpaired e⁻): 0.75
Cu spin density (%): 45.5
N_α spin density (%): 21.1
C_{Ar} spin density (%): 4.3

d-orbital occupancy:
α: 0.98, 0.99, 0.99, 0.99, 0.99
β: **0.58**, 0.94, 0.96, 0.98, 0.99

$[Cu(4H^+/12e^-)]^{1-}_{D2d}$ (3)
d(Cu···N_α) (Å): 1.96
d(N_α···C_{Ar}) (Å): 1.36
d(C_{Ar}···C_{Ar}) (Å): 1.41
<S^2> (unpaired e⁻): 0.00
Cu spin density (%): 2.0
N_α spin density (%): 35.1
C_{Ar} spin density (%): 40.5

d-orbital occupancy:
α: 0.84, 0.91, 0.98, 0.98, 0.99
β: 0.83, 0.94, 0.95, 0.97, 0.99

$[Cu(4H^+/11e^-)]^{0}_{D2d}$ (4)
d(Cu···N_α) (Å): 1.96
d(N_α···C_{Ar}) (Å): 1.34
d(C_{Ar}···C_{Ar}) (Å): 1.41
<S^2> (unpaired e⁻): 0.75
Cu spin density (%): 21.3
N_α spin density (%): 32.4
C_{Ar} spin density (%): 13.7

d-orbital occupancy:
α: 0.94, 0.94, 0.97, 0.97, 0.98
β: 0.87, 0.91, 0.93, 0.93, 0.95

$[Cu(4H^+/10e^-)]^{1+}_{D2d}$ (5)
d(Cu···N_α) (Å): 1.97
d(N_α···C_{Ar}) (Å): 1.32
d(C_{Ar}···C_{Ar}) (Å): 1.42
<S^2> (unpaired e⁻): 0.00
Cu spin density (%): 0.0
N_α spin density (%): 0.0
C_{Ar} spin density (%): 0.0

d-orbital occupancy:
α: 0.93, 0.93, 0.95, 0.95, 0.96
β: 0.93, 0.93, 0.95, 0.95, 0.96

Figure 4. (A) Summary of the characterization of complexes **2**, **3**, **4**, and **5**. (B) DFT calculations on the electronic structure of complexes **2**, **3**, **4**, and **5** (see the SI for details on the calculations of the complexes in different geometries and spin states).

plot (no spin density in the ligand or the metal ion) and the d-orbital occupancy (d^{10}) were consistent with a Cu^I ion bound by two quinone-like ligands, $[(^qLH_2)_2Cu^I]^{1+}$.

Overall, the spectroscopic and computational evidence suggest the involvement of ligand-based redox processes in the oxidation of complex **2** to **5** (Figure 4A). Paradoxically, the lower oxidation state (**2**) is a Cu^{II} complex while the highest oxidation state (**5**) is formally a Cu^I complex. This behavior is paradigmatic of metal complexes bound by redox-active ligands and has a direct impact on the reactivity of this species: complex **2** is O_2 sensitive, as opposed to most Cu^{II} complexes, and complex **5** is not oxidized by O_2, as opposed to most Cu^I complexes.

Reactivity with Proton/Electron Donors and Acceptors. The stoichiometric conversion between complex **1** and complex **5** was carried out in DMF using H^+/e^- donors and acceptors with varying bond dissociation free energy (Figure 5).[22] We have recently reported that "high-valent" CuOH intermediates perform the $2H^+/2e^-$ oxidation of 2,6-di-*tert*-butylphenol (2,6-DTBP; $BDFE_{O-H}^{DMSO}$ = 76.7 kcal/mol[1,23,24]) via formation of a fleeting phenoxyl radical (2,6-DTBP•) that undergoes dimerization to the corresponding diphenol (H_2DPQ) before being oxidized to 3,3′,5,5′-tetra-*tert*-butyldiphenoquinone (DPQ, see Figure 6A).[25] The reaction of **5** with 2,6-DTBP was followed by ^{1}H-NMR (Figure 6B), and we observed that the $4H^+/4e^-$ reduction of **5** produced Cu^I and 2 equiv of $^{cat}LH_4$ (complex **1** in 99% yield),

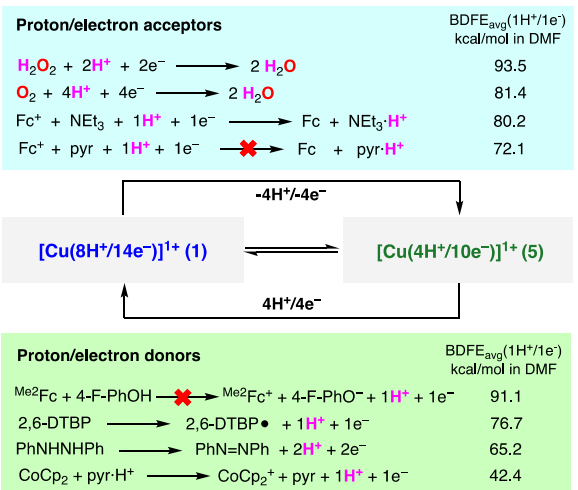

Figure 5. Reactivity of the $4H^+/4e^-$ ECPB system **1**/**5** toward H^+/e^- acceptors (top) and H^+/e^- donors (bottom).[22]

with DPQ as the main phenol oxidation product (95% yield). The ECPB mass balance ([**1**] + [**5**]) remained above 70% throughout the reaction.

Complex **5** was also quantitatively reduced to **1** using other $2H^+/2e^-$ donors (e.g., diphenylhydrizine, PhNHNHPh; see section 5 of the SI) and combinations of acids and $1e^-$

https://doi.org/10.1021/jacs.2c05454
J. Am. Chem. Soc. 2022, 144, 16905−16915

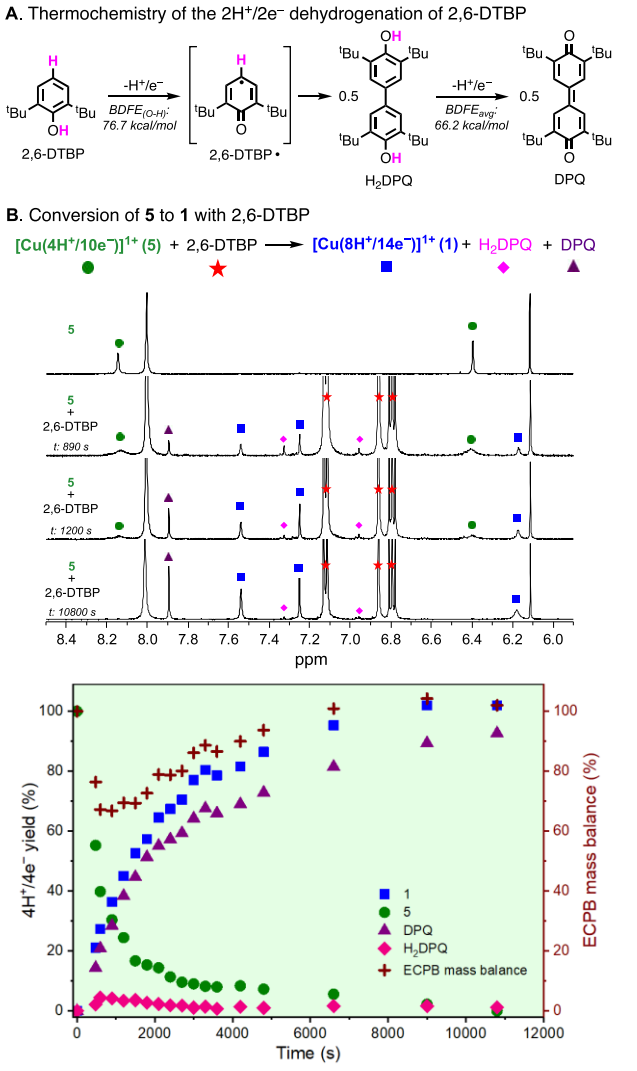

Figure 6. (A) Thermochemistry of the $2H^+/2e^-$ dehydrogenation of 2,6-DTBP. (B) Stoichiometric $4H^+/4e^-$ reductive protonation of complex **5** to **1** with 2,6-DTBP followed by ^{1}H-NMR.[25]

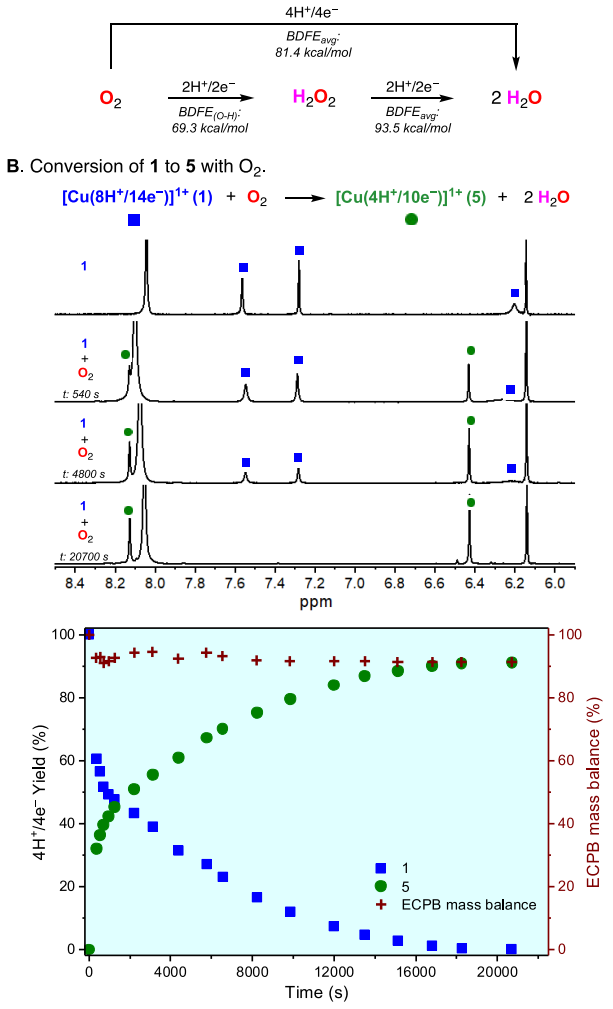

Figure 7. (A) Thermochemistry for the $4H^+/4e^-$ reductive protonation of dioxygen. (B) Stoichiometric $4H^+/4e^-$ oxidative deprotonation of complex **1** to complex **5** with O_2 followed by ^{1}H-NMR.

reductants (Figure 5). For example, stoichiometric amounts of pyridinium triflate (pyr·H^+) and cobaltocene ($CoCp_2$) reduced **5** to **1** (yield: 99%), but the use of a weaker acid (4-fluorophenol, 4-F-PhOH) and a weaker reductant (dimethylferrocene, Me_2Fc) did not.

Complex **5** did not react with substrates containing weak C−H bonds such as xanthene ($BDFE_{C-H}^{DMSO}$ = 70.2 kcal/mol), 9,10-dihydroanthracene ($BDFE_{C-H}^{DMSO}$ = 72.9 kcal/mol), and 9-fluorene ($BDFE_{C-H}^{DMSO}$ = 74.3 kcal/mol) despite having similar bond dissociation free energy (BDFE) to the phenols oxidized by complex **5** (e.g., 2,6-DTBP, $BDFE_{O-H}^{DMSO}$ = 76.7 kcal/mol). It has long been determined that O−H bonds undergo H-atom abstraction more quickly than C−H bonds, and it is predicted that at the same driving force ($BDFE_{C-H} = BDFE_{O-H}$), O−H bonds react 10,000 times faster than C−H bonds.[26]

As we mentioned, the oxidative deprotonation of **1** to **5** can be coupled with the reduction of O_2 to H_2O (Figure 7A). This reaction was also followed by ^{1}H-NMR (Figure 7B), and we observed that the $4H^+/4e^-$ oxidative deprotonation of complex **1** produced complex **5** in remarkable yields (91%) and maintained an ECPB mass balance above 90% during the oxygenation. In the oxidation of complex **1** to **5** with O_2, H_2O_2 was not formed (the ^{1}H-NMR peak at 11 ppm corresponding to H_2O_2 was not observed). In fact, the $4H^+/4e^-$ transformation of complex **1** to **5** could also be accomplished using stoichiometric amounts H_2O_2 ($2H^+/2e^-$ acceptor, 70% yield). While the reaction of **1** with O_2 to produce complex **5** was slow (hours), the reaction between **1** and H_2O_2 was extremely fast (minutes). These results suggest that the reaction between **1** and O_2 could potentially lead to the formation of H_2O_2, but its accumulation in solution is precluded.

The oxidative deprotonation of **1** to **5** could also be performed using combinations of $1e^-$ oxidants and bases (see section 4.2 of the SI).[22] For example, addition of ferrocenium (Fc^+) and triethylamine (NEt_3) to a DMF solution of **1** produced **5** in good yields. Conversely, complex **5** was not formed when Fc^+ and pyridine (weaker base than NEt_3) were used.

To support that the Cu system could be used as a buffer for protons and electrons, we reacted equimolar mixtures of **1** and **5** with H^+/e^- donors (e.g., $CoCp_2$/pyr·H^+, PhNHNHPh, and so forth) and H^+/e^- acceptors (e.g., Fc^+/NEt_3, H_2O_2) in a substoichiometric fashion (see section 4.3 of the SI). In all of

https://doi.org/10.1021/jacs.2c05454
J. Am. Chem. Soc. 2022, 144, 16905−16915

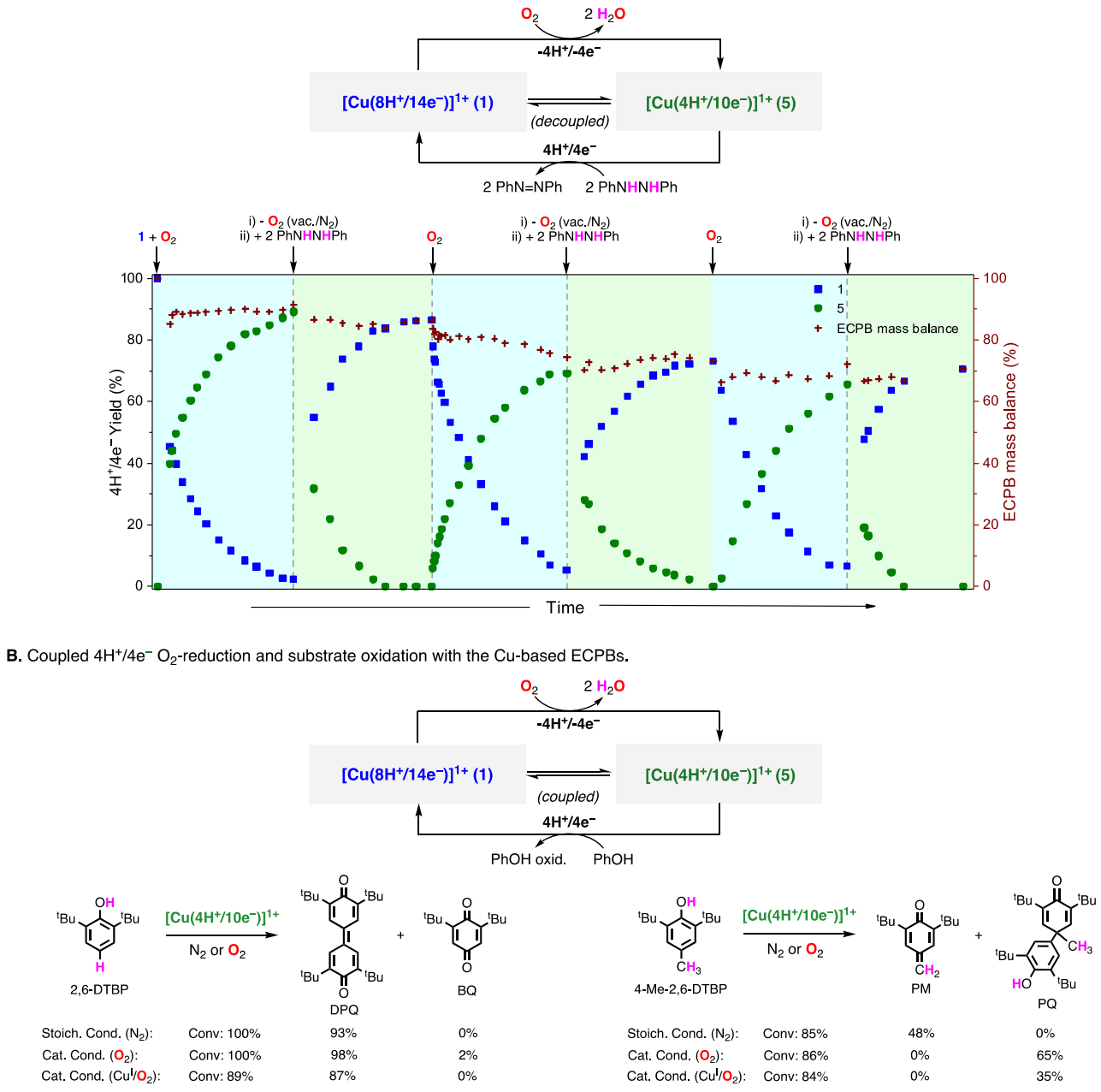

Figure 8. (A) Decoupling O_2-reduction and substrate oxidation with the **1**/**5** ECPB system. (B) Coupling O_2-reduction and substrate oxidation with the **1**/**5** ECPB system.

the cases, the **1**/**5** equilibrium was maintained with good ECPB mass balance and for reactants with a wide range of pK_a's, $E_{1/2}$, and BDFEs (see the SI).

Decoupled O_2-Reduction and Substrate Oxidation with the ECPB. By definition, ECPB systems capture and deliver H_2 equivalents (i.e., protons and electrons) in a decoupled and reversible fashion.[12] To demonstrate that our ECBP system was capable of performing such transformations, we used **1**/**5** to decouple the reductive protonation of O_2 with the oxidative deprotonation of PhNHNHPh (Figure 8A). During the first oxidative cycle, oxygenation of **1** (followed by NMR) produced **5** in remarkable yields (90%). After full consumption of **1**, the excess of O_2 was removed and 2 equiv of PhNHNHPh were added. During this first reductive cycle, we observed that complex **5** was stoichiometrically converted to complex **1** with concomitant formation of 2 equiv of PhN═NPh.

The second oxidative cycle was then carried out by bubbling O_2 in the DMF-d_7 solution containing complex **1** and PhN═NPh, which regenerated complex **5** with good yields (75%). Removal of O_2 and addition of PhNHNHPh initiated the second reductive cycle, which produced **1** and PhN═NPh. A third oxidative cycle (addition of O_2) and a third reductive cycle (addition of PhNHNHPh after removal of O_2) were performed, and the ECPB mass balance was maintained above 70% (each of the oxygenation cycles led to a reduction of the ECPB mass balance of 10%). To the best of our knowledge, this constitutes one of the first examples of a metal complex capable of decoupling the reductive protonation of O_2 with the

https://doi.org/10.1021/jacs.2c05454
J. Am. Chem. Soc. 2022, 144, 16905−16915

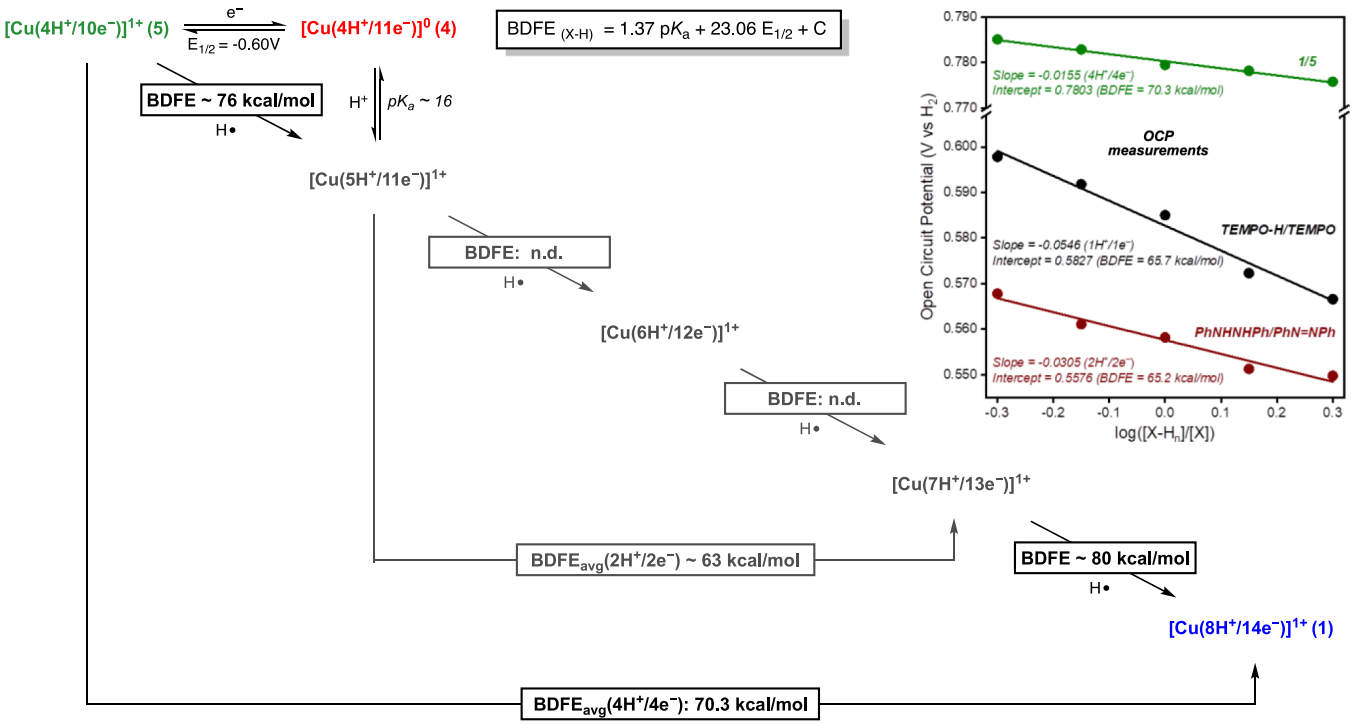

Figure 9. BDFE calculations for the $1H^+/1e^-$ protonation/reduction of **5** using the Bordwell equation (top left) and determination of the $BDFE_{avg}$ for the $4H^+/4e^-$ conversion between **1** and **5** determined using open circuit potential measurements (OCP, see top right).

oxidative deprotonation of organic substrates in multiple cycles.

Stoichiometric and Catalytic Oxidation of Phenols. The ECPB system could also be used in the coupled oxidation of 4-X-2,6-DTBPs with O_2 (Figure 8B). Complex **5** (10 mol %) catalyzed the aerobic oxidation of 2,6-DTBP to DPQ with remarkable conversion and selectivity (100% conv., 99% yield). Oxidation of 4-Me-2,6-DTBP under stoichiometric anaerobic conditions (uncoupled oxidation) and catalytic aerobic conditions (coupled oxidation) led to different oxidation products. While under anaerobic conditions the quinone methide dehydrogenation product was obtained (PM in Figure 8B), under catalytic aerobic conditions, the C−C coupling product 2,6-di-*tert*-butyl-4-methyl-4-(3,5-di-*tert*-butyl-4-hydroxyphenyl)-2,5-cyclohexadien-l-one (PQ in Figure 8B) was formed (see the SI for details on the product analysis). The slow reactivity of the PhOH substrates did not allow for uncoupling the reduction of O_2 with the oxidation of these substrates (like we have done with PhNHNHPh) because full conversion of complex **5** to **1** required excess amounts of phenol, (phenol substrates are oxidized by combining copper(I) and dioxygen without redox-active ligand). These background catalytic reactions ($Cu^I + O_2$ + PhOH) were also analyzed, and we observed the formation of the same phenol oxidation products (DPQ for 2,6-DTBP and PQ for 4-Me-2,6-DTBP) but with poorer substrate conversion, product selectivity, and yields, suggesting that complex **5** is the main active oxidant in the coupled oxidations catalyzed by the ECPB system.

Many Cu complexes catalyze the aerobic oxidation of phenols, but reports on the Cu-catalyzed oxidation of 4-substituted 2,6-di-tert-butylphenols are scarce.[27] For 4-Me-2,6-DTBP, it has been found that the utilization of Cu salts (e.g., $CuCl_2$) and simple bidentate ligands (e.g., morpholine, ethylenediamine) produced several oxidation products (poor selectivity), and the formation of the quinone methide product (PM) was postulated but could not be observed.[28,29] These precedents clearly differ from our findings, in which complex **5** could generate selectively PM or PQ only by varying the reaction conditions (i.e., decoupled stoichiometric oxidation under N_2 or coupled catalytic oxidation under O_2).

Determination of the Bond Dissociation Free Energies in the ECPB. All of the reactivity results described above indicate that the oxidative deprotonation of **1** requires proton/electron acceptors capable of oxidizing X−H bonds with a BDFE higher than 80 kcal/mol (Figure 9). By combining $1e^-$ oxidants and bases, which act together as H-atom acceptors, we determined that the BDFE for the $1H^+/1e^-$ deprotonation/oxidation of **5** had a value between 80.2 kcal/mol (complex **1** was oxidized by NEt_3 and Fc^+, which have a $BDFE_{eff}$ of 80.2 kcal/mol) and 79.6 (complex **1** was not oxidized by proton sponge and Fc^+, which have a $BDFE_{eff}$ of 79.6 kcal/mol).

The reactivity experiments suggest that complex **5** is capable of abstracting H-atoms from substrates with BDFEs lower than 77 kcal/mol (e.g., 2,6-DTBP). Combinations of acids and reductants, which can act as H-atom donors, were used to determine the BDFE for this $1H^+/1e^-$ process. Complex **5** was reduced by Me_2Fc/4-NO_2-PhOH ($BDFE_{eff}$ of 72.9 kcal/mol) but was not reduced by $Me_{10}Fc$/4-NO_2-PhOH ($BDFE_{eff}$ of 82.2 kcal/mol) and was partially reduced by Me_2Fc/4-NO_2−2,6-DTBP ($BDFE_{eff}$ of 76.7 kcal/mol), indicating that the BDFE for the $1H^+/1e^-$ reductive protonation of complex **5** is close to 76 kcal/mol. We were also able to determine the BDFE for the $1H^+/1e^-$ reduction of **5** with the $E_{1/2}$ of the **4**/**5** couple (−0.60 V vs $Fc^{0/+}$) and the pK_a for the protonation of **4** (ca. 16 in DMF) using the Bordwell equation (BDFE = 76 kcal/mol, see Figure 9; Note: the protonation of **4** was irreversible but the pK_a could be estimated using acids with different strength, see the SI).

https://doi.org/10.1021/jacs.2c05454
J. Am. Chem. Soc. 2022, 144, 16905−16915

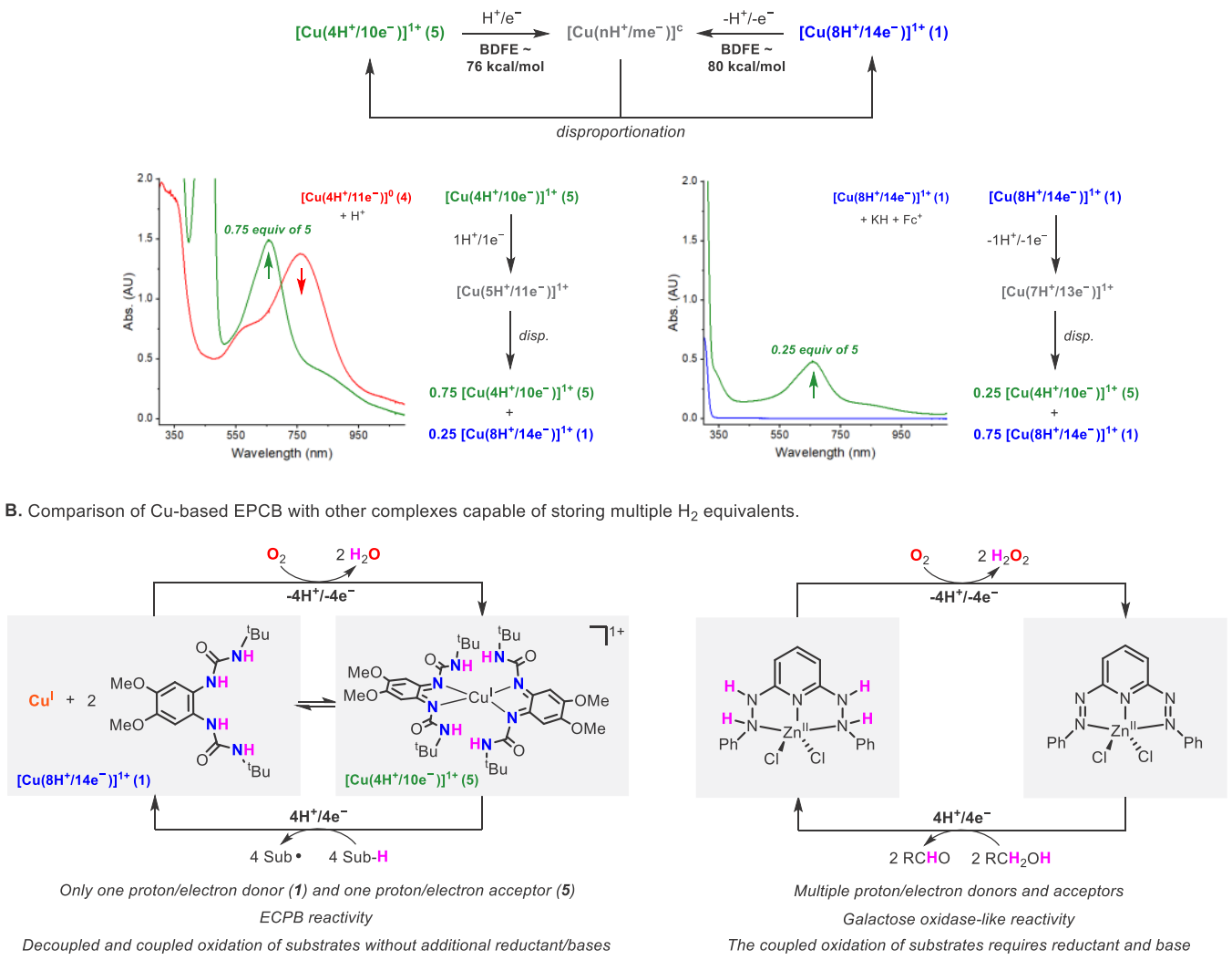

Figure 10. (A) Stoichiometry of the disproportionation reactions observed upon $1H^+/1e^-$ protonation/reduction of **5** and $1H^+/1e^-$ deprotonation/oxidation of **1** that led to ECBP regeneration. (B) Comparison of the reactivity of the Cu-based ECPB system described in this article with other metal complexes capable of performing multiproton multielectron transformations (e.g., Zn complex reported by Goswami and coworkers[32]).

Following the protocol recently described by Mayer and coworkers, we determined the $BDFE_{avg}$ for the $4H^+/4e^-$ conversion between **1** and **5** (See Figure 9 inset).[30] Open circuit potential (OCP) measurements using different ratios of **1** and **5** in a NEt_3/NEt_3H^+ buffer in DMF showed Nernstian dependence with a slope of −0.0155, confirming that the transformation between **1** and **5** involves 4 protons and 4 electrons (Note: In these OCP measurements, the ideal slope should be −0.059 for $1H^+/1e^-$ processes, −0.0295 for $2H^+/2e^-$ processes, and −0.01475 for $4H^+/4e^-$ processes). To validate our results, we carried out OCP measurements for PhNHNHPh/PhN═NPh mixtures ($2H^+/2e^-$, slope = −0.0305) and TEMPO/TEMPO-H mixtures (TEMPO-H: 2,2,5,5-tetramethyl-N-hydroxy-piperidine; $1H^+/1e^-$, slope = −0.0546) under the same conditions.

The $BDFE_{avg}$ for the $4H^+/4e^-$ reductive protonation of **1** to **5** was 70.3 kcal/mol (see the SI for details on the calculations). Taking into account the BDFE value for the $1H^+/1e^-$ reductive protonation of **5** (76 kcal/mol) and the BDFE value for the $1H^+/1e^-$ oxidative deprotonation of **1** (80 kcal/mol), we can estimate that two of the intermediate protonation/oxidation states between **1** and **5** ($[\mathbf{Cu(5H^+/11e^-)}]^{1+}$ and $[\mathbf{Cu(6H^+/12e^-)}]^{1+}$ (see Figure 9) are poor proton/electron acceptors ($BDFE_{avg}$ for the $2H^+/2e^-$ reduction of $[\mathbf{Cu(5H^+/11e^-)}]^{1+}$ is 63 kcal/mol).

Mechanism of Regeneration of the ECPB in the Protonation/Reduction and Deprotonation/Oxidation Reactions. The protonation of complex **4** with 4-NO_2−2,6-DTBP (4-nitro-2,6-di-*tert*-butylphenol; pK_a^{DMF}: 8.3[23,31]) resulted in the formation of **5** and **1** via disproportionation. The stoichiometry for this disproportionation process (formation of 0.75 equiv of **5** and 0.25 equiv of **1**) was obtained by determining the concentrations of **5** and **1** by UV−vis and ^{1}H-NMR (Figure 10A, see also SI). The $1H^+/1e^-$ oxidative deprotonation of complex **1** was carried out using 1 equiv of KH and 1 equiv of Fc^+, leading also to the formation of **1** and **5**. UV−vis and NMR experiments confirmed that this disproportionation process produced 0.25 equiv of **5** and 0.75 equiv of **1**. The ability of this Cu-based system to undergo clean and fast disproportionation reactions to selectively

https://doi.org/10.1021/jacs.2c05454
J. Am. Chem. Soc. 2022, 144, 16905−16915

produce **1** and **5** upon reduction/protonation of **5** and deprotonation/oxidation of **1** is critical to explain its ECPB reactivity (Figure 10A). When we followed the reaction between **5** and proton/electron donors (e.g., 2,6-DTBP), and the reaction between **1** and proton/electron acceptors (e.g., O_2), no Cu species other than **1** and **5** were observed (see the SI). This suggests that the protonation/oxidation states between **1** and **5** are less stable than **1** and **5**, the latter being thermodynamic sinks (Figure 10A). These results are in agreement with the thermodynamic analysis described above which suggests that the ECPB reactivity of the Cu-based systems relies on the oxidative power of complex **5** and the strength of the N−H bonds in complex **1** (i.e., the reductive protonation of complex **5** leads to the formation of good proton/electron donors that will disproportionate to produce strong N−H bonds in complex **1**).

Mechanistic Discussion. The $4H^+/4e^-$ conversion of O_2 to H_2O is a thermodynamically favored process ($-\Delta G^\circ$ = 324.7 kcal/mol), but the reactivity of O_2 with most organic molecules is kinetically disfavored because of its triplet spin state and the poor driving force of the $1H^+/1e^-$ reduction of O_2 to hydroperoxyl ($HO_2^{\cdot}$), associated with the low bond dissociation free energy of the O−H bond formed ($BDFE_{(O-H)}$: 51.2 kcal/mol).[1] The **1**/**5** ECPB system allows for harnessing the $4H^+/4e^-$ oxidative of power of O_2 in a single oxidant, complex **5**, which is formed via the oxidative deprotonation of **1** and regenerated via disproportionation after undergoing reductive protonation. We believe that copper plays a critical role in this ECPB system, stabilizing the "high-valent" complex **5** (Cu^I center bound by four imine ligands in a pseudo-tetrahedral geometry) and promoting O_2 reduction in complex **1** (Note: Mn^{II}, Fe^{II}, Co^{II}, Ni^{II}, and Zn^{II} did not lead to $^{cat}LH_4$ oxidation when exposed to O_2).

The reactivity of the Cu-based ECPB systems described herein differs from most of the metal complexes capable of reversibly accumulating H-atom and H_2 equivalents in their structure (Figure 10B).[33−35] Many of the complexes that perform multiproton multielectron transformations (see Zn example in Figure 10B[32]) rely on the formation of multiple protonation/oxidation states and the coordination of the organic substrates prior to oxidation (e.g., most of these systems mimic the reactivity of galactose oxidase, which carries out the aerobic dehydrogenation of alcohols to aldehydes upon alkoxide coordination[36,37]), and their ability to act as ECPBs was not reported.

CONCLUSIONS

We believe that the findings described in this article will inspire the development of other metal-based ECPB systems capable of promoting multiproton multielectron transformations. We are currently working on studying the kinetics of the interconversion between **1** and **5** with different proton/electron donors and acceptors to determine if the reaction rates are dependent on the thermodynamic driving force of these transformations (i.e., difference in BDFE between the H-atom donor and acceptor) or if other factors should be considered (e.g., identity of the bonds formed and broken, difference between the pK_a or $E_{1/2}$ of the acceptor and donor, etc.). By modifying the ligand scaffold and/or the metal ion, we envision that ECPBs capable of promoting multiproton multielectron transformations that require low BDFEs (e.g., N_2/NH_3 interconversion) or high BDFEs (e.g., dehydrogenation of strong C−H bonds) will be developed, and some of them will be utilized in electrochemical and/or photochemical devices for reversible H_2 abstraction, storage, and delivery.[33,38]

ASSOCIATED CONTENT

Supporting Information

The Supporting Information is available free of charge at https://pubs.acs.org/doi/10.1021/jacs.2c05454.

Experimental details, including characterization data, spectra, reactivity studies, computations, and crystallographic data for **5** and **2** (CCDC number: 2173659 and 2173660) (PDF)

Accession Codes

CCDC 2173659−2173660 contain the supplementary crystallographic data for this paper. These data can be obtained free of charge via www.ccdc.cam.ac.uk/data_request/cif, or by emailing data_request@ccdc.cam.ac.uk, or by contacting The Cambridge Crystallographic Data Centre, 12 Union Road, Cambridge CB2 1EZ, UK; fax: +44 1223 336033.

AUTHOR INFORMATION

Corresponding Authors

Marcel Swart − *University of Girona, IQCC, 17003 Girona, Spain; ICREA, 08010 Barcelona, Spain;* orcid.org/0000-0002-8174-8488; Email: marcel.swart@udg.edu

Michael P. Hendrich − *Department of Chemistry, Carnegie Mellon University, Pittsburgh, Pennsylvania 15213, United States;* orcid.org/0000-0003-4775-0389; Email: hendrich@andrew.cmu.edu

Isaac Garcia-Bosch − *Department of Chemistry, Carnegie Mellon University, Pittsburgh, Pennsylvania 15213, United States;* orcid.org/0000-0002-6871-3029; Email: igarciab@andrew.cmu.edu

Authors

Tong Wu − *Department of Chemistry, Carnegie Mellon University, Pittsburgh, Pennsylvania 15213, United States*

Khashayar Rajabimoghadam − *Department of Chemistry, Southern Methodist University, Dallas, Texas 75275, United States*

Ankita Puri − *Department of Chemistry, Carnegie Mellon University, Pittsburgh, Pennsylvania 15213, United States*

David D. Hebert − *Department of Chemistry, Carnegie Mellon University, Pittsburgh, Pennsylvania 15213, United States;* orcid.org/0000-0003-3999-7904

Yi Lin Qiu − *Department of Chemistry, Carnegie Mellon University, Pittsburgh, Pennsylvania 15213, United States*

Sidney Eichelberger − *Department of Chemistry, Southern Methodist University, Dallas, Texas 75275, United States*

Maxime A. Siegler − *Johns Hopkins University, Baltimore, Maryland 21218, United States;* orcid.org/0000-0003-4165-7810

Complete contact information is available at: https://pubs.acs.org/10.1021/jacs.2c05454

Author Contributions

The manuscript was written through contributions of all authors. All authors have given approval to the final version of the manuscript.

Notes

The authors declare no competing financial interest.

https://doi.org/10.1021/jacs.2c05454
J. Am. Chem. Soc. 2022, 144, 16905−16915

■ ACKNOWLEDGMENTS

We thank the Robert A. Welch Foundation (grant N-1900-20190330 to I.G.B.), the National Science Foundation (Grant No. [1941220] to I.G.B.), AEI/MCIU (PID2020-114548GB-I00 to M.S.), and FEDER (UNGI10-4E-801 to M.S.) for financial support. Research reported in this publication was supported by the National Institute of General Medical Sciences of the National Institutes of Health under Award Number R35GM137914 (to I.G.B.) and Award Number R35GM141948 (to M.P.H.). The content is solely the responsibility of the authors and does not necessarily represent the official views of the National Institutes of Health.

■ REFERENCES

(1) Agarwal, R. G.; Coste, S. C.; Groff, B. D.; Heuer, A. M.; Noh, H.; Parada, G. A.; Wise, C. F.; Nichols, E. M.; Warren, J. J.; Mayer, J. M. Free Energies of Proton-Coupled Electron Transfer Reagents and Their Applications. *Chem. Rev.* **2022**, *122*, 1−49.

(2) Nocera, D. G. Proton-Coupled Electron Transfer: The Engine of Energy Conversion and Storage. *J. Am. Chem. Soc.* **2022**, *144*, 1069−1081.

(3) Thammavongsy, Z.; Mercer, I. P.; Yang, J. Y. Promoting proton coupled electron transfer in redox catalysts through molecular design. *Chem. Commun.* **2019**, *55*, 10342−10358.

(4) Yoshikawa, S.; Shimada, A. Reaction Mechanism of Cytochrome c Oxidase. *Chem. Rev.* **2015**, *115*, 1936−1989.

(5) McEvoy, J. P.; Brudvig, G. W. Water-Splitting Chemistry of Photosystem II. *Chem. Rev.* **2006**, *106*, 4455−4483.

(6) Qing, G.; Ghazfar, R.; Jackowski, S. T.; Habibzadeh, F.; Ashtiani, M. M.; Chen, C.-P.; Smith, M. R.; Hamann, T. W. Recent Advances and Challenges of Electrocatalytic N2 Reduction to Ammonia. *Chem. Rev.* **2020**, *120*, 5437−5516.

(7) Lubitz, W.; Reijerse, E. J.; Messinger, J. Solar water-splitting into H2 and O2: design principles of photosystem II and hydrogenases. *Energy Environ. Sci.* **2008**, *1*, 15−31.

(8) Smith, K. W.; Stroupe, M. E. Mutational Analysis of Sulfite Reductase Hemoprotein Reveals the Mechanism for Coordinated Electron and Proton Transfer. *Biochemistry* **2012**, *51*, 9857−9868.

(9) Van Eerden, F. J.; Melo, M. N.; Frederix, P. W. J. M.; Periole, X.; Marrink, S. J. Exchange pathways of plastoquinone and plastoquinol in the photosystem II complex. *Nat. Commun.* **2017**, *8*, 15214.

(10) Rochaix, J.-D. Regulation of photosynthetic electron transport. *Biochim. Biophys. Acta* **2011**, *2011*, 375−383.

(11) Anson, C. W.; Stahl, S. S. Mediated Fuel Cells: Soluble Redox Mediators and Their Applications to Electrochemical Reduction of O_2 and Oxidation of H_2, Alcohols, Biomass, and Complex Fuels. *Chem. Rev.* **2020**, *120*, 3749−3786.

(12) Symes, M. D.; Cronin, L. Decoupling hydrogen and oxygen evolution during electrolytic water splitting using an electron-coupled-proton buffer. *Nat. Chem.* **2013**, *5*, 403−409.

(13) Rausch, B.; Symes, M. D.; Cronin, L. A Bio-Inspired, Small Molecule Electron-Coupled-Proton Buffer for Decoupling the Half-Reactions of Electrolytic Water Splitting. *J. Am. Chem. Soc.* **2013**, *135*, 13656−13659.

(14) Zhang, F.; Wang, Q. Redox-Mediated Water Splitting for Decoupled H2 Production. *ACS Mater. Lett.* **2021**, *3*, 641−651.

(15) Liu, W.; Mu, W.; Deng, Y. High-Performance Liquid-Catalyst Fuel Cell for Direct Biomass-into-Electricity Conversion. *Angew. Chem., Int. Ed.* **2014**, *53*, 13558−13562.

(16) Rajabimoghadam, K.; Darwish, Y.; Bashir, U.; Pitman, D.; Eichelberger, S.; Siegler, M. A.; Swart, M.; Garcia-Bosch, I. Catalytic Aerobic Oxidation of Alcohols by Copper Complexes Bearing Redox-Active Ligands with Tunable H-Bonding Groups. *J. Am. Chem. Soc.* **2018**, *140*, 16625−16634.

(17) Rajabimoghadam, K.; Darwish, Y.; Bashir, U.; Pitman, D.; Eichelberger, S.; Siegler, M. A.; Garcia-Bosch, I. Tunable intramolecular multicenter H-bonding interactions in first-row metal complexes bearing bidentate redox-active ligands. *J. Coord. Chem.* **2019**, *72*, 1346−1357.

(18) Cheng, H.-Y.; Tzeng, B.-C.; Peng, S.-M. Synthesis and crystal structure of [CuI(N-ch-bqdi)2]Cl (N-ch-bqdi = N-cyclohexyl-benzoquinodiimine). A novel d10 benzoquinonediimine complex. *Bull. Inst. Chem. Acad. Sin.* **1994**, *41*, 51−60.

(19) Ye, S.; Sarkar, B.; Lissner, F.; Schleid, T.; van Slageren, J.; Fiedler, J.; Kaim, W. Three-Spin System with a Twist: A Bis(semiquinonato)copper Complex with a Nonplanar Configuration at the Copper(II) Center. *Angew. Chem., Int. Ed.* **2005**, *44*, 2103−2106.

(20) Kaim, W. Manifestations of Noninnocent Ligand Behavior. *Inorg. Chem.* **2011**, *50*, 9752−9765.

(21) Sit, P. H. L.; Car, R.; Cohen, M. H.; Selloni, A. Simple, Unambiguous Theoretical Approach to Oxidation State Determination via First-Principles Calculations. *Inorg. Chem.* **2011**, *50*, 10259−10267.

(22) The bond dissociation free energy (BDFE) measures the strength of an X−H bond in a specific solvent (see ref. 1). The minimum energy required to break homolytically the O−H bond in 2,6-di-*tert*-butylphenol to form the corresponding phenoxyl radical (2,6-DTBP -> 2,6-DTBP· + H·) is 76.7 kcal/mol in DMSO. BDFEs are also useful to analyze reactions involving the transfer of multiple H atoms ($BDFE_{avg}$, see ref. 1). For example, the $4H^+/4e^-$ oxidation of water to dioxygen ($2\ H_2O$ -> O_2 + 4 H·) has a free energy per H atom transferred of 81.4 kcal/mol in DMF. This value is not the average of the O−H bonds since it also includes the O−O double bond cleavage. This value reflects the BDFE required for an H-atom donor to give isoergic conversion of O_2 to H_2O. The same thermochemical analysis can be done for combinations of acid/reductant and oxidant/base. The combination of ferrocenium and pyridine could break X−H bonds homolytically as strong as 81.6 kcal/mol in DMF in an isoergic fashion (see SI for further details).

(23) Bordwell, F. G.; Zhang, X.-M. Acidities and homolytic bond dissociation enthalpies of 4-substituted-2,6-di-tert-butylphenols. *J. Phys. Org. Chem.* **1995**, *8*, 529−535.

(24) We estimate that the $BDFE_{X-H}$ values are similar in DMF and DMSO. See SI for further details.

(25) Wu, T.; MacMillan, S. N.; Rajabimoghadam, K.; Siegler, M. A.; Lancaster, K. M.; Garcia-Bosch, I. Structure, Spectroscopy, and Reactivity of a Mononuclear Copper Hydroxide Complex in Three Molecular Oxidation States. *J. Am. Chem. Soc.* **2020**, *142*, 12265−12276.

(26) Mayer, J. M. Understanding Hydrogen Atom Transfer: From Bond Strengths to Marcus Theory. *Acc. Chem. Res.* **2011**, *44*, 36−46.

(27) Allen, S. E.; Walvoord, R. R.; Padilla-Salinas, R.; Kozlowski, M. C. Aerobic Copper-Catalyzed Organic Reactions. *Chem. Rev.* **2013**, *113*, 6234−6458.

(28) Orlando, C. M. Cuprous chloride-amine catalyzed oxidation of 2,6-di-tert-butyl-p-cresol with oxygen. *J. Org. Chem.* **1968**, *33*, 2516−2518.

(29) Hewitt, D. G. The copper−amine catalysed autoxidation of phenols. Part I. *J. Chem. Soc. C: Org.* **1971**, 2967−2973.

(30) Wise, C. F.; Agarwal, R. G.; Mayer, J. M. Determining Proton-Coupled Standard Potentials and X−H Bond Dissociation Free Energies in Nonaqueous Solvents Using Open-Circuit Potential Measurements. *J. Am. Chem. Soc.* **2020**, *142*, 10681−10691.

(31) Maran, F.; Celadon, D.; Severin, M. G.; Vianello, E. Electrochemical determination of the p*K*a of weak acids in N,Ndimethylformamide. *J. Am. Chem. Soc.* **1991**, *113*, 9320−9329. Note: The p*K*a of the acids/bases in DMF was estimated using their p*K*a in DMSO with the formula: $pK_a(DMF) = 1.56 + 0.96*pKa(DMSO)$. See SI for further details

(32) Pramanick, R.; Bhattacharjee, R.; Sengupta, D.; Datta, A.; Goswami, S. An Azoaromatic Ligand as Four Electron Four Proton Reservoir: Catalytic Dehydrogenation of Alcohols by Its Zinc(II) Complex. *Inorg. Chem.* **2018**, *57*, 6816−6824.

https://doi.org/10.1021/jacs.2c05454
J. Am. Chem. Soc. 2022, 144, 16905−16915

(33) Anferov, S. W.; Czaikowski, M. E.; Anderson, J. S. Metal−ligand cooperative transfer of protons and electrons. *Trends Chem.* **2021**, *3*, 993−996.
(34) Cattaneo, M.; Ryken, S. A.; Mayer, J. M. Outer-Sphere 2 e−/2 H+ Transfer Reactions of Ruthenium(II)-Amine and Ruthenium(IV)-Amido Complexes. *Angew. Chem., Int. Ed.* **2017**, *56*, 3675−3678.
(35) Du, H.-Y.; Chen, S.-C.; Su, X.-J.; Jiao, L.; Zhang, M.-T. Redox-Active Ligand Assisted Multielectron Catalysis: A Case of CoIII Complex as Water Oxidation Catalyst. *J. Am. Chem. Soc.* **2018**, *140*, 1557−1565.
(36) Whittaker, M. M.; Whittaker, J. W. Catalytic Reaction Profile for Alcohol Oxidation by Galactose Oxidase. *Biochemistry* **2001**, *40*, 7140−7148.
(37) Wang, Y.; DuBois, J. L.; Hedman, B.; Hodgson, K. O.; Stack, T. D. P. Catalytic Galactose Oxidase Models: Biomimetic Cu(II)-Phenoxyl-Radical Reactivity. *Science* **1998**, *279*, 537−540.
(38) Pannwitz, A.; Wenger, O. S. Proton-coupled multi-electron transfer and its relevance for artificial photosynthesis and photoredox catalysis. *Chem. Commun.* **2019**, *55*, 4004−4014.

https://doi.org/10.1021/jacs.2c05454
J. Am. Chem. Soc. 2022, 144, 16905−16915